Journal of the Korean Nuclear Society
Volume 26, Number 3, September 1994

Study of the Secondary Flow Effect on the Turbulent Flow Characteristics in Fuel Rod Bundles

Kye-Bock Lee, Ho-Cheol Jang, and Sang-Keun Lee
Korea Atomic Energy Research Institute
(Received January 7, 1994)

핵연료봉 주위의 난류 유동장 특성에 미치는 이차 유동의 영향에 대한 연구

이계복 · 장호철 · 이상근
한국원자력연구소
(1994. 1. 7 접수)

Abstract

Numerical predictions including secondary flows have been performed for fully developed turbulent single-phase rod bundle flows. The $k-\varepsilon$ turbulence model(two equation model) for the isotropic eddy viscosity, together with an algebraic stress model for generating secondary velocities, enabled the prediction of mean axial velocities, secondary velocities, and turbulent kinetic energy and turbulent stresses.

Comparisons with experiment have shown that the influence of secondary motion on mean flow and turbulence is clearly evident. The convective transport effects of secondary flow on the velocity field have been identified.

요 약

수치 해석을 통하여 이차 유동을 포함한 핵연료봉 주위의 난류 유동장을 예측하였다. 등방성 난류 와점성계수 모델과 이차 유동을 모사하기 위해 단순화된 대수응력모델을 사용하여 난류 운동 에너지(k)와 난류 에너지 소멸률(ε)의 이 방정식 모델과 운동량 방정식을 유한 차분법으로 풀어 유동장내의 평균 속도, 이차유동, 난류 운동 에너지, 난류 응력 분포 등을 구하였다. 수치해석 예측치를 실험데이타와 비교하여 만족할만한 결과를 얻었고 유동장 내에서 이차 유동의 영향을 확인하였다. 즉 이차 유동이 절대 크기는 작더라도 대류 효과에 의해 큰 영향을 미치는 것을 본 연구를 통해 알 수 있었다.

1. Introduction

Most nuclear reactor cores contain a large number of fuel rods arranged in either square or equilateral triangular pitched arrays over which the coolant flows axially. The prediction of fuel rod clad temperature is important to the safe and economic operation of nuclear reactor core. The thermal-hydraulic performance of rod bundle is related to the turbulent flow structure through the process of crossflow mixing,

since this mixing provides a mechanism to equalize coolant temperature. Thus, the structure of axially developed turbulent flow through large regularly spaced rod arrays is of considerable importance to the design and analysis of the thermal-hydraulics of nuclear power reactor core. Accurate calculation of temperature fields requires detailed knowledge of the velocity fields in subchannels, which is difficult due to the complexity of the turbulence phenomena.

The main source of information on turbulent flow structure is experiment where, in some cases, detailed measurements of turbulence have been made. Experimental investigations all yielded mean flow and turbulence distributions with distortions. These characteristics are much influenced by the turbulence-driven secondary flows that occur in the cross-plane of all non-circular passages. These flows cause the main flow to spiral through the passage and, although they are relatively weak compared with the main flow, they have a significant influence on the local mean flow distributions of interest, chiefly the axial velocity, wall shear stress and turbulent kinetic energy.

Most attempts to measure turbulence-driven secondary flows in rod bundles were not successful either due to geometrical tolerances of the test sections which caused crossflow or due to experimental accuracy. Although Trupp and Azad[1] could infer the direction and approximate magnitude of secondary flows from momentum and energy balances, they were unable to measure the tiny secondary velocities via hot wire. Similarly, Carajilescov and Todreas[2] and Rowe[3] lacked sufficient resolution to extract secondary velocities from measurements with their laser doppler systems. Kjellström[4] obtained some hot wire data for the peripheral components of secondary velocitiy. Whereas the results strongly indicated the existence of secondary motion, the large scatter did not permit definite conclusion to be drawn even with the data uniformly shifted to remove a possible systematic error. Secondary flows have been shown to exist in non-circular channels by Launder and Ying[5] for a square duct and by Aly et al[6]. for a triangular duct. The unique feature of all ducts for which experimental data have been obtained is that these ducts have corners in their shape. Vonka[7] reported experimental data on secondary flows for a triangular array. He found that the magnitude of the secondary flow velocity is less than 0.1% of the axial velocity. In reality, he measured crossflow velocities of the order of 1% of the axial velocity which were caused by crossflow from the inner subchannels into the outer ones due to not fully developed flow and also due to the blockage of the outer subchannels by the spacers. This blockage causes a crossflow into the inner subchannels at the spacer level which downstream of the spacer redistributes.

Detailed velocity and temperature distributions within rod bundles have recently been predicted by solving the basic differential equations of turbulent flow and energy. Considerable difficulties were encountered with convergence of the solutions due mainly to the coupling and non-linearity of the equations, a feature that was most prominent in the cross-plane Reynolds stress. The most widely used procedure has been based on the $k-\varepsilon$ turbulence model for the effective viscosity, together with a model for the cross plane Reynolds stress that allows the small but significant secondary velocities to be generated. However, the results of these applications have often proved inadequate and contradictory, and the lacks of high-quality experimental measurements of the turbulence structure in rod bundles have inhibited the development of the turbulence models. Therefore in most cases, secondary flow was neglected and anisotropic eddy viscosities were introduced to improve the circumferential coupling of the velocity. Thus, early attempts to solve these equations for rod bundle flows involved many simplications including ignoring cross-plane flows or allowing indirectly in some way for their effects, the latter being typically the use of anisotropic turbulent viscosities or prescribed wall shear stress distribution.

Two approaches for including anisotropic nature are suggested in the literature[8, 9]

1) correlate the anisotropic factor with other turbulent quantities
2) correlate the anisotropic factor with locations of interest

The second approach is usually employed because of its simplicity. The bases of adjusting the function for the anisotropy factor are the distributions of axial velocity and wall shear stress. The anisotropic character of turbulent flow adapted to the $k-\varepsilon$ equation model of turbulence improves the prediction of flow and heat transfer characteristics inside the subchannels of an infinite rod array.

The anisotropy factor for turbulent flow in rod bundles is suggested by numerous investigators. Thus there are many functions of anisotropy factor reported[10]. Some calculation method[10] based on this anisotropy factor has been successfully developed for the prediction of mean flow characteristics. But, the predictions of turbulent flow obtained by Bartzis and Todreas[11], Seale[12] were found to be unacceptable and eventually in both cases secondary flows were omitted and a one dimensional velocity field was calculated using prescribed anisotropic turbulent viscosities-presumably-to compensate for the lack of secondary motions. Bartzis and Todreas also tried to unsuccessfully to obtain acceptable secondary velocity fields with the empirical stress descriptions. It appears that the calculation methods using anisotropic eddy viscosities and neglecting secondary flow may be mainly compensating for the neglect of convection transport rather than allowing for any anisotropy in diffusion transport. So far, it is evident that the various levels of success obtained in the previous predictions indicates that a procedure based on the Launder and Ying's[13] algebraic stress model for the cross plane stresses coupled with the $k-\varepsilon$ turbulence model is likely to provide a useful approach. Trupp and 'Aly[8] obtained a reasonable secondary flow field in a triangular subchannel using a Launder and Ying's model. But they were apparently unable to obtain satisfactory convergence of solution without an immutable sign restriction on the vorticity source term. Therefore, the direction of the secondary flow circulation was prescribed in order to obtain reasonable convergence of the solution.

From the above summary, it will be apparent that the situation for calculating fully developed three dimensional turbulent velocity fields in rod bundles is confused with, as yet, no convincing general prediction method available. The generality of each method reported so far has been compromised to a greater or lesser extent by the simplification to or restriction of the governing equations solved and/or by significant input of special empirical data such as turbulent length scale. To predict the turbulent and secondary flow exactly, simplified algebraic versions of the Reynolds stress transport equations must be used in the calculation of the full three dimensional velocity field without any special adjustments for each geometry.

The objectives of this study are to develop the turbulent model without any special adjustments for each geometry and reveal the significant role of the cross plane turbulence-driven secondary flow.

2. Mathematical and Physical Model

2.1. Governing Equations

Consider an infinite equilateral triangular array of rods with the primary flow parallel to the rods. A primary flow cell for such an array is shown in Fig. 1 together with the cylindrical polar coordinates system (r, θ, z) used in the study.

To predict the flow characteristics, the fundamental physical laws of continuity and momentum conservation are employed with transport equations of turbulent kinetic energy k and turbulent dissipation rate ε. The mathematical representation of these equations of an incompressible, constant fluid property, steady state, fully developed flow can be written

as follows:

−continuity

$$\frac{1}{r}\frac{\partial(rV_r)}{\partial r}+\frac{1}{r}\frac{\partial V_\theta}{\partial\theta}=0 \tag{1}$$

−momentum

$$\frac{1}{r}\frac{\partial(\rho rV_rV_z)}{\partial r}+\frac{1}{r}\frac{\partial(\rho V_\theta V_z)}{\partial\theta}=-\frac{\partial P}{\partial z}+\frac{1}{r}\frac{\partial}{\partial r}$$
$$[r(\mu_t+\mu)\frac{\partial V_z}{\partial r}]+\frac{\partial}{r\partial\theta}[\frac{1}{r}(\mu_t+\mu)\frac{\partial V_z}{\partial\theta}] \tag{2}$$

$$\frac{1}{r}\frac{\partial(\rho rV_rV_r)}{\partial r}+\frac{1}{r}\frac{\partial(\rho V_\theta V_r)}{\partial\theta}=-\frac{\partial P}{\partial r}+\frac{1}{r}\frac{\partial}{\partial r}$$
$$[r(\mu\frac{\partial V_r}{\partial r}-\rho\overline{v_r^2})]+\frac{\partial}{r\partial\theta}(\frac{\mu}{r}\frac{\partial V_r}{\partial\theta}-\rho\overline{v_rv_\theta})+\rho\frac{V_\theta^2}{r}$$
$$-\frac{\mu V_r}{r^2}-\frac{2\mu}{r^2}\frac{\partial V_\theta}{\partial\theta}+\rho\frac{\overline{v_\theta^2}}{r} \tag{3}$$

$$\frac{1}{r}\frac{\partial(\rho rV_rV_\theta)}{\partial r}+\frac{1}{r}\frac{\partial(\rho V_\theta V_\theta)}{\partial\theta}=-\frac{\partial P}{r\partial\theta}+\frac{1}{r}\frac{\partial}{\partial r}$$
$$[r(\mu\frac{\partial V_\theta}{\partial r}-\rho\overline{v_rv_\theta})]+\frac{\partial}{r\partial\theta}(\frac{\mu}{r}\frac{\partial V_\theta}{\partial\theta}-\rho\overline{v_\theta^2})-\frac{\rho V_rV_\theta}{r}$$
$$-\frac{\mu V_\theta}{r^2}+\frac{2\mu}{r^2}\frac{\partial V_r}{\partial\theta}-\frac{\rho\overline{v_rv_\theta}}{r} \tag{4}$$

−turbulent kinetic energy

$$\frac{1}{r}\frac{\partial(\rho rV_rk)}{\partial r}+\frac{1}{r}\frac{\partial(\rho V_\theta k)}{\partial\theta}$$
$$=\frac{1}{r}\frac{\partial}{\partial r}[r(\frac{\mu_t}{\sigma_k}+\mu)\frac{\partial k}{\partial r}]+\frac{\partial}{r\partial\theta} \tag{5}$$
$$[\frac{1}{r}(\frac{\mu_t}{\sigma_k}+\mu)\frac{\partial k}{\partial\theta}]+\mu_t\left(\frac{\partial V_z}{\partial r}\right)^2+\mu_t\left(\frac{\partial V_z}{r\partial\theta}\right)^2-\rho\varepsilon$$

−turbulent dissipation rate

$$\frac{1}{r}\frac{\partial(\rho rV_r\varepsilon)}{\partial r}+\frac{1}{r}\frac{\partial(\rho V_\theta\varepsilon)}{\partial\theta}$$
$$=\frac{1}{r}\frac{\partial}{\partial r}[r(\frac{\mu_t}{\sigma_\varepsilon}+\mu)\frac{\partial\varepsilon}{\partial r}]+\frac{\partial}{r\partial\theta}$$
$$[\frac{1}{r}(\frac{\mu_t}{\sigma_\varepsilon}+\mu)\frac{\partial\varepsilon}{\partial\theta}]+f_1C_{\varepsilon1}P'\frac{\varepsilon}{k}-\rho f_2C_{\varepsilon2}\frac{\varepsilon^2}{k} \tag{6}$$

$$P'=\mu_t\left(\frac{\partial V_z}{\partial r}\right)^2+\mu_t\left(\frac{\partial V_z}{r\partial\theta}\right)^2$$

where

$$\sigma_k=1.0 \quad \sigma_\varepsilon=1.34 \quad C_{\varepsilon1}=1.55 \quad C_{\varepsilon2}=2.0$$

−Launder and Ying's model

$$\overline{v_z^2}=C_1k \tag{7}$$

$$\overline{v_r^2}=C_3k-C_2C_4\frac{k^3}{\varepsilon^2}\left(\frac{\partial V_z}{\partial r}\right)^2 \tag{8}$$

$$\overline{v_\theta^2}=C_3k-C_2C_4\frac{k^3}{\varepsilon^2}\left(\frac{\partial V_z}{r\partial\theta}\right)^2 \tag{9}$$

$$\overline{v_rv_\theta}=-C_2C_4\frac{k^3}{\varepsilon^2}\left(\frac{\partial V_z}{\partial r}\right)\left(\frac{\partial V_z}{r\partial\theta}\right) \tag{10}$$

$$\overline{v_rv_z}=-C_4\frac{k^2}{\varepsilon}\left(\frac{\partial V_z}{\partial r}\right) \tag{11}$$

$$\overline{v_\theta v_z}=-C_4\frac{k^2}{\varepsilon}\left(\frac{\partial V_z}{r\partial\theta}\right) \tag{12}$$

where

f_1 and f_2 are turbulence model functions for wall effect.

The turbulent components of the stresses in the above equations were calculated with the algebraic stress model of Launder and Ying[13] to yield explicit relations for all components of the turbulent stress tensor. The simplification of the Reynolds stress transport equations removed the partial differential stress terms and enabled Launder and Ying to derive algebraic relations for the cross plane stresses. This algebraic stress transport model was first derived for square duct calculations and further analyzed to yield a set of algebraic equations for the complete Reynolds stress tensor in terms of axial velocity gradients, turbulence kinetic energy k and its dissipation rate ε. The empirical constants in the stress model were adjusted to match the predicted mean flow distribution with experiment, which were mainly within the error band of their measurements, showed distortions in axial velocity and wall shear stress distribution that attributed to secondary flow.

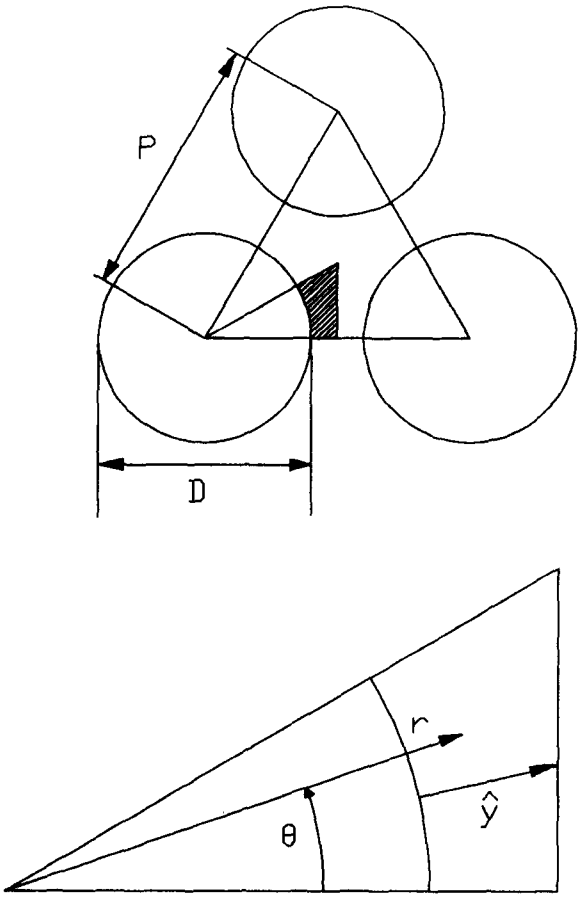

Fig. 1. Subchannel of Triangular Array and Notation of Coordinates

The turbulent eddy viscosity is related to the local values of the turbulent kinetic energy and turbulent dissipation rate by the Prandtl-Kolmogorov formula,

$$\nu_t = f_\mu C_\mu \frac{k^2}{\varepsilon} \tag{13}$$

where C_μ is 0.085 and f_μ is turbulence model function.

2.2. Numerical Scheme

The governing equations were solved by finite difference method on a mesh of orthogonally intersecting grid lines. The well-known EL−2D computer program, used as the framework for present calculations, employs the SIMPLER solution algorithm of Patankar[14].

A staggered mesh was employed with cross-plane velocities located at main control volume face intersections with the main grid lines and the continuity equation was manipulated into an equation for pressure correction so that "SIMPLER" method could be used for solution of cross-plane momentum and continuity.

The number of grid points for each subchannel depends on the pitch-to-diameter ratio and the arrangement of rod arrays. If equal radial mesh increments were used, the very high velocity gradients in the laminar sublayer adjacent to the rod surface would require a fine mesh spacing in this region. This mesh, however, cannot be extended over the whole calculation area owing to the large number of velocity points created. Thus, a logarithmic radial mesh spacing was used. The spacing of this mesh was determined by the wall friction velocity and rod gap distance. The matching of the cylindrical geometry radial mesh to the subchannel center straight line boundary was achieved by creating an additional radial mesh circle for the intersection of each of the angular mesh lines outside the rod-gap line. The computations for several grid systems were performed to compare the prediction results and computation time. Finally the 33×17 grid system was selected in the present computation and shown in Fig. 2.

The convergence criteria used was the ratio of the updated values calculated for each variable to the previous values to below 10^{-3}.

2.3. Boundary Conditions

The boundaries of the solution domain consist of three straight lines of geometry symmetry and a sector of circular curve. The boundary nodes next to the surfaces at $\theta = 0°$ and $\theta = 30°$ are easy to handle be-

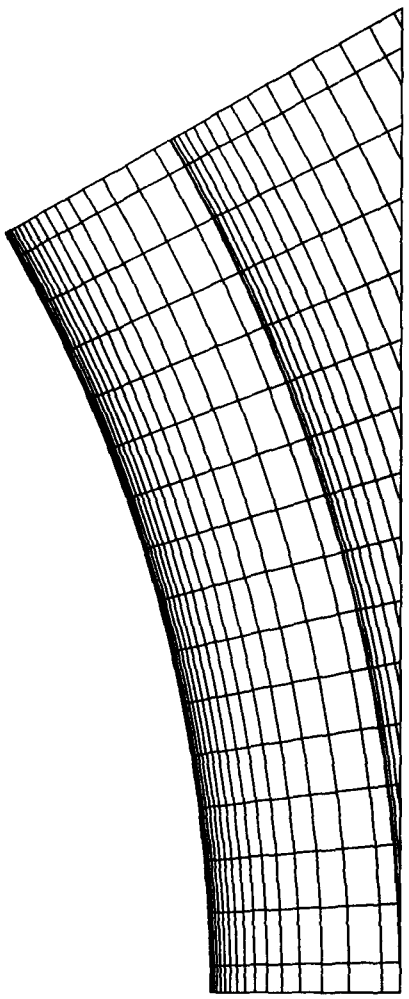

Fig. 2. Main Grid System: P/D=1,123

cause of the symmetric nature of the geometry. The presence of the wall ensures that over a finite region of the flow, however thin, the turbulence Reynolds number is low enough for molecular viscosity to influence directly the process of production, dissipation and transport of turbulence. These viscous interactions render the problem of creating a general mathematical model of the turbulence at least an order of magnitude more difficult than for high Reynolds number flows. Wall functions, based on the notion of one dimensional local equilibrium conditions, were conventionally used to bridge between the interior solution and the boundary surfaces. But, in this study, the turbulence kinetic energy and its dissipation is very sensitive to the node distance next to the wall. Therefore, the low Reynolds number model developed by Lam et al.[16] for wall flows is employed. This model does not require the use of wall function formulas and does not require the introduction of additional terms into the transport equations.

In governing equations, f_1, f_2 and f_μ have been proposed to account for wall effect as follows;

$$f_1 = 1 + \left(\frac{A_{c1}}{f_\mu}\right)^3$$

$$f_2 = 1 - e^{R_t^2}$$

$$f_\mu = (1 - e^{-A_\mu R_k})^2 (1 + \frac{A_1}{R_t}) \qquad (14)$$

where $A_\mu = 0.0165, \quad A_1 = 20.5, \quad A_{c1} = 0.05$

$$R_k = \frac{k^{1/2} y}{\nu}, \quad R_t = \frac{k^2}{\nu \varepsilon}$$

The three boundaries of the calculation mesh not adjacent to a rod wall from reflection boundaries to the velocity solution, with a zero velocity gradient across them, and the velocity of the fluid at the rod surface is zero.

At the symmetry boundaries, the normal gradients of k and ε will be zero and at the wall, the normal gradient of ε and turbulent kinetic energy are zero.

3. Results and Discussion

For laminar flow conditions, the momentum equation can be solved analytically for the flow through the fuel bundle array[16]. The finite difference equation approximation to the momentum equation, and the associated numerical mesh, were used to solve the laminar flow. This was carried out as a means of testing the stability, the adequacy of

boundary condition and accuracy of the numerical mesh, since the logarithmically spaced radial mesh coupled with the matching of the cells to the subchannel center line creates very substantial changes in the radial mesh spacing.

The predicted mean axial velocity profiles plotted in Fig. 3 are in fair good agreement with the analytical solution. Also shown in Fig. 4 is the wall shear stress profile, which is of the same shape to the analytical solution.

The detailed results of prediction using the isotropic turbulent modelling with secondary flow are compared and discussed against the experimental data of Carajilescov and Todreas[2] with P/D ratio of 1.123 and $Re = 2.7 \times 10^4$.

The comparison of the mean axial velocity contours between experimental and computational results are shown in Fig. 5. The comparison shows excellent agreement in the major part of the subchannel. Predictions with secondary flow suppressed are also given where their effects were strong. The contours show the characteristic

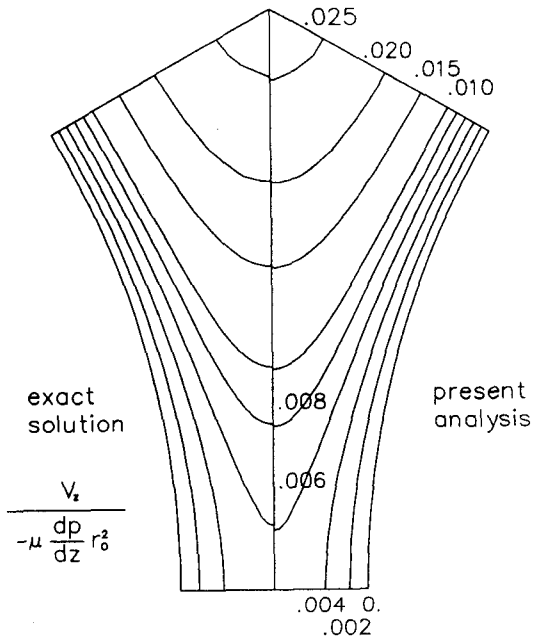

Fig. 3. Predicted and Exact Axial Velocity Contours for Laminar Flow: P/D=1.1, Re=80

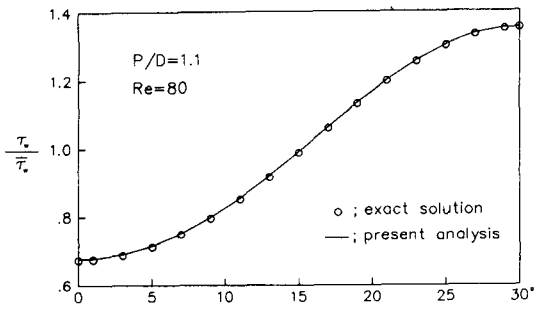

Fig. 4. Distribution of the Wall Shear Stress for Laminar Flow

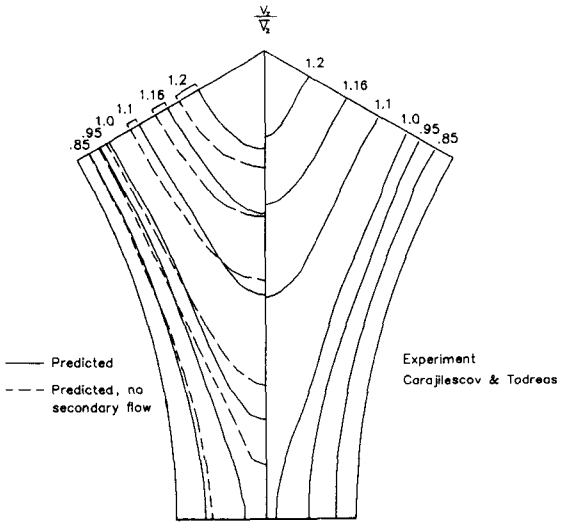

Fig. 5. Axial Velocity Contours (Re=27,000 P/D=1.123)

influences of the secondary flow with significant bulging into the gap region, due to the convective transport of core fluid in that direction.

Fig. 6 represents wall shear stress profiles. Comparing predictions with and without secondary flow modeling, the wall shear stress is seen to be increased near the gap region and decreased near the subchannel center by secondary flow. This is interpreted as the convective effects of fluid which will increase axial velocity gradients in the near wall wall region at lower θ and decrease them at higher θ. This tendency illustrates the remarkable effect of sec-

ondary flow in homogenizing the wall shear stress. The influence of secondary flow on the wall shear stress is more markedly than that on the mean axial velocity.

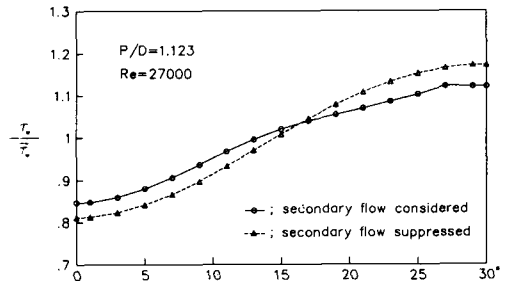

Fig. 6. Distribution of the Wall Shear Stress of Triangular Subchannel

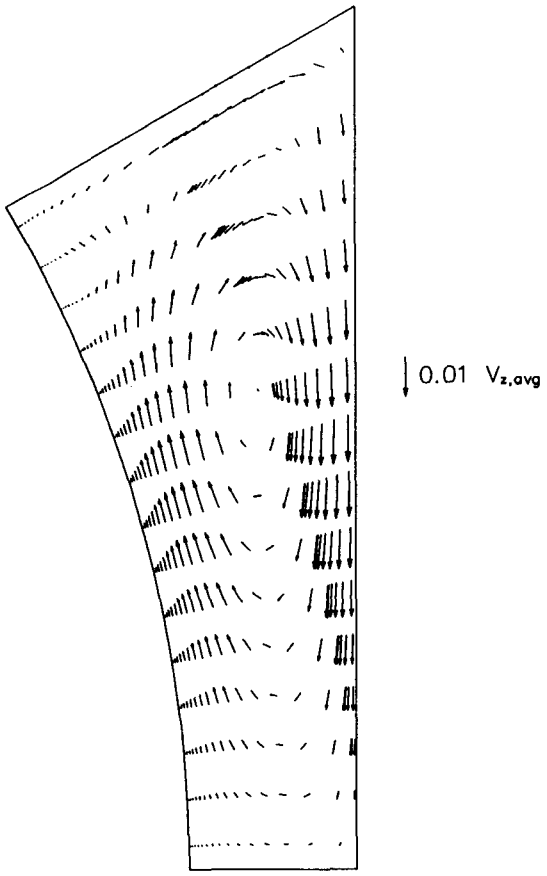

Fig. 7. Predicted Secondary Velocity Profiles of Triangular Subchannel: P/D=1.123, Re=27,000

A single swirl of secondary flow was predicted for this case as seen in Fig. 7. It seems that the flow consists of single cell of circulation in which high momentum fluid from the subchannel center to the gap region with return flow along the wall surface. This pattern is similar to the measurements of Trupp et al.[6] for equilateral triangular duct. The maximum secondary velocities were about 1% of the mean axial velocity.

The predicted contours of turbulent kinetic energy is shown in Fig. 8. The distortions due to secondary flow is markedly. The agreement with the experimental data is reasonable.

All components of the normal Reynolds stresses are shown in Fig. 9. They were normalized by the mean axial velocity. Predicted Reynolds stress profiles compared with experiment are generally the same shape and trends.

4. Conclusion

Fully developed turbulent flow through equilateral triangular array fuel bundles has been investigated

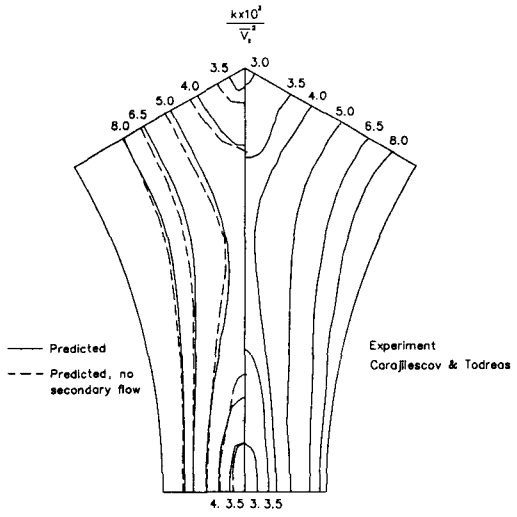

Fig. 8. Turbulent Kinetic Energy Contours (Re=27,000, P/D=1.123)

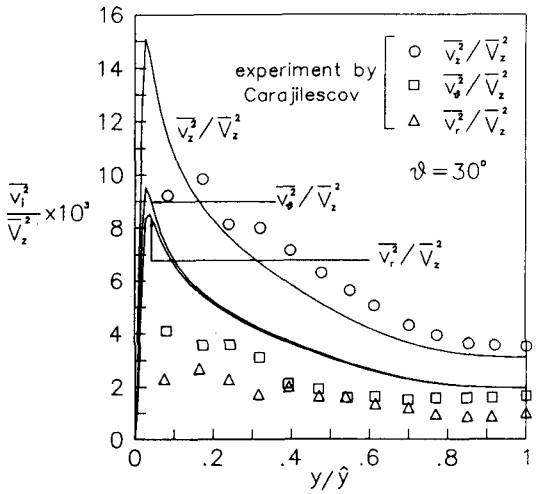

Fig. 9. Turbulent Normal Stress Distribution of Triangular Subchannel: P/D=1.123, Re=27,000

numerically. The flow is much influenced by the turbulence-driven secondary flows that occur in the cross plane of all non-circular passages.

The $k-\varepsilon$ turbulence model employing the isotropic eddy viscosity, together with an algebraic stress model has been used. The present method has retained the generality without any compromise by prescribing the direction of secondary flow or restricting the governing equations solved. The experimental and predicted characteristics of the flow are shown to be in good agreement.

The effect of secondary flow is evident on the mean axial velocity, turbulent kinetic energy and wall shear stress distributions. It acts to homogenize the wall shear stress along the rod surface by increasing the velocity gradients near the gap.

Previous calculation methods using anisotropic eddy viscosity and neglecting secondary flow were successful in predicting the mean flow characteristics. But, this is mainly compensating for the neglect of convection transport rather than allowing for any anisotropy in diffusion transport. The secondary flow and anisotropy phenomena are physically different, but they are not completely independent. Secondary flows arise mainly due to anisotropy in the Reynolds stresses, but they, in turn, influence the the distribution of shear stress in the fluid. Therefore, it seems that turbulent diffusion and secondary flow convection are of importance in momentum transport.

To comprehend the true role and importance of the secondary flow, more experimental study on anisotropy factor and secondary flow distribution should be performed.

Nomenclature

A_1, $A_{\mu 1}$	constants in the turbulence model functions
C_1, C_2, C_3, C_4	constants in the turbulent stress model
$C_{\varepsilon 1}$, $C_{\varepsilon 2}$	constants in the turbulence model
C_μ	constant in the turbulent viscosity
D	rod diameter
f_1, f_2, f_μ	turbulence model functions for wall effect
k	turbulence kinetic energy
P	rod pitch
r, θ z	cylindrical corodinates
R	Reynolds number
V_i	mean velocity component in the direction i
v_i	fluctuating component of velocity in the direction i
y	distance from rod to point of interest in the radial direction
$\hat{y}$	distance from wall to maximum velocity line
ε	dissipation rate of turbulence kinetic energy
σ_k, σ_ε	turbulent Prandtl number
μ	laminar viscosity
μ_t	turbulent viscosity
ν_t	kinematic turbulent viscosity

References

1. A.C. Trupp and R.S. Azad, "The structure of

Turbulent Flow in Triangular Array Rod Bundles," Nuclear Engineering and Design, Vol. 32, pp 47−84, 1975

2. P. Carajilescov and N.E. Todreas, "Experimental and Analytical Study of Axial Turbulent Flows in an Interior Subchannel of a Bare Rod Bundle," ASME, J. Heat Transfer, Vol. 98, pp 262−268, 1976
3. D.S. Rowe, Measurement of Turbulent Velocity, Intensity and Scale in Rod Bundle Flow Channels, BNWL-1736, Battelle Pacific Northwest Laboratories, 1973
4. B. Kjellström, Studies of Turbulent Flow Parallel to a Rod Bundle of Triangular Array, AE−487, Aktiebolaget Atomenergi, 1971
5. B.E. Launder and W.M. Ying, "Secondary Flows in Ducts of Square Cross-Section," Journal of Fluid Mechanics, Vol. 54, pp 289−295, 1972
6. A.M.M. Aly, A.C. Trupp and A.D. Gerrard, "Measurements and Prediction of Fully Developed Turbulent Flow in an Equilateral Triangular Duct," Journal of Fluid Mechanics, Vol. 85, pp 57−83, 1978
7. V. Vonka, "Turbulent Transports by Secondary Flow Vortices in a Rod Bundle," Nuclear Engineering and Design, Vol. 106, pp 209−220, 1988
8. A.C. Trupp and A.M.M. Aly, "Predicted Secondary Flows in Triangular Array Rod Bundles," ASME, J. Fluids Engrg., Vol. 101, pp 354−363, 1979
9. C.W. Rapley, "The Simulation of Secondary Flow Effects in Turbulent Non-Circular Passage Flows," Int. J. Numerical Methods in Fluids, Vol. 2, pp 331−347, 1982
10. A.S. Yang and C.C. Chieng, "Turbulent Heat and Momentum Transports in an Infinite Rod Array," ASME, J. Heat Transfer, Vol. 109, pp 599−605, 1987
11. J.G. Bartzis and N.E. Todreas, "Turbulence Modeling of Axial Flow in a Bare Rod Bundle," ASME, J. Heat Transfer, Vol. 101, pp 628−634, 1979
12. W.J. Seale, "Measurements and Prediction of Fully Developed Turbulent Flow in a Simulated Rod Bundle," Journal of Fluid Mechanics, Vol. 123, 399−423, 1982
13. B.E. Launder and W.M. Ying, "Prediction of Flow and Heat Transfer in Ducts of Square Cross Section," Proceedings of the Institution of Mechanical Engineers, Vol. 187, pp 455−463, 1973
14. S.V. Patankar, Numerical Heat Transfer and Fluid Flow, Hemisphere Publishing Co., 1980
15. C.G.K. Lam and K. Bremhorst, "A Modified Form of the $k-\varepsilon$ Model for Predicting Wall Turbulence," ASME J. Fluids Engrg., Vol. 103, 456−460, 1981
16. E.M. Sparrow and A.L. Loeffler, Jr., "Longitudinal Laminar Flow Between Cylinders Arranged in Regular Array," AIChE Journal, Vol. 5, 325−330, 1959